CHINA FOUNDRY Research & Development
Vol.16 No.1 January 2019
https://doi.org/10.1007/s41230-019-8113-y

Evolution of interfacial dislocation networks during long term thermal aging in Ni-based single crystal superalloy DD5

Qiang Gao[1], *Li-rong Liu[1], Xiao-hua Tang[1], Zhi-jiang Peng[2], Ming-jun Zhang[2], and Su-gui Tian[1]

1. School of Materials Science and Engineering, Shenyang University of Technology, Shenyang 110870, China

2. AECC Shenyang Liming Aero Engine Co. Ltd., Shenyang 110043, China

Abstract: Interfacial dislocations found in single crystal superalloys after long term thermal aging have an important effect on mechanical properties. Long term thermal aging tests for DD5 single crystal superalloy were carried out at 1,100 °C for 20, 100, 200, 500 and 1000 h, and then cooled by air. The effect of long term thermal aging on the dislocation networks at the *γ*/*γ*′ interfaces was investigated by FE-SEM. Results showed that during the long term thermal aging at 1,100 °C, misfit dislocations formed firstly and then reorientation in the (001) interfacial planes occurred. Different types of square or rectangular dislocation network form by dislocation reaction. Square dislocation networks consisting of four groups of dislocations can transform into octagonal dislocation networks, and then form another square dislocation network by dislocation reaction. Rectangular dislocation networks can also transform into hexagonal dislocation networks. The interfacial dislocation networks promote the *γ*′ phase rafting process. The dislocation networks spacings become smaller and smaller, leading to the effective lattice misfit increasing from –0.10% to –0.32%.

Key words: DD5 single crystal superalloy; interfacial dislocations; long term thermal aging; effective lattice misfit

CLC numbers: TG132.3$^+$3 **Document code:** A **Article ID:** 1672-6421(2019)01-014-09

Ni-based single crystal superalloys used as turbine blades for aircraft and gas turbine engines are strengthened by a high volume fraction of γ' precipitates, coherently embedded in the disordered γ matrix [1-3]. During high temperature service, the γ/γ' microstructure degradation of Ni-based superalloys has a great influence on the rafting process and mechanical properties [4,5]. Therefore, it is important to investigate the impact of growth and coarsening behavior of γ' precipitates on microstructural stability of single crystal superalloys. Interfacial dislocations have been found in single crystal superalloys after long term thermal aging by TEM [6-8], which has an important effect on the mechanical properties. The interfacial dislocation networks are produced by misfit strains during long term aging at zero stress. There exsit other kinds of dislocation networks, which are produced during creep testing, such as reactangular and hexgonal dislocation networks [9]. All the above dislocation networks in superalloys are produced by a/2<110> dislocations [10-11]. TEM is a universal tool that can be applied to observe dislocations and identify their line vectors and Burgers vectors. However, the TEM method has several disadvantages in some respects: small area of investigation, which is critical for investigation inhomogeneous materials, especially for superalloys with dendritic segregation; it is difficult to observe three-dimensional (3D) imaging of dislocations configurations; and, it is time consuming to prepare the specimen, etc. Epishin et al. [12,13] firstly used SEM to investigate the dislocations after creep tests, which overcame the above shortcomings and fully showed the superiority of SEM observation. SEM can be used to observe the dislocation patterns in the whole specimen and infer the dislocation moving direction by the contrast [12]. More importantly, we can judge whether the dislocation is from dislocation reaction by the contrast in the image by SEM or not [12]. However, as described in Ref. [13], for the observation of interfacial dislocation in SEM, two experimental aspects have to be considered: the test temperature must be high enough to dissolve a

***Li-rong Liu**

Female, born in 1976, Ph.D, Associate Professor. Research interest: microstructure and properties of superalloy.

E-mail: lrliu@sut.edu.cn

Received: 2018-08-30; Accepted: 2018-12-11

part of γ′ sufficient for groove formation (about 2%), and the cooling rate should be slow enough for the groove to form but fast enough to avoid network distortion. Our experiments met the above conditions.

The aim of the present work is to investigate the evolution of interfacial dislocation networks during long term thermal aging by FE-SEM in DD5 single crystal superalloy. The effective lattice misfit parameters were also estimated by measuring the dislocation network spacing.

1 Experimental procedure

Experiments were performed using the second generation Ni-based single crystal superalloy DD5. The nominal chemical composition of the alloy is Ni-7.5Co-7Cr-1.5Mo-5W-6.2Al-6.5Ta-3Re-0.15Hf (wt.%). Samples were provided by Shenyang Liming Aero Engine Co., Ltd. in fully heat treated conditions (i.e. solution heat treatment under vacuum for 2 h at 1,300 °C/pulsed air cooling + 4 h at 1,100 °C/air cooling + 16 h at 870 °C/air cooling). DD5 single crystal rods have a close [001] crystallographic orientation. Long term thermal aging tests were carried out at 1,100 °C for 20, 100, 200, 500 and 1,000 h, and then cooled by air. Samples for SEM observation were cut perpendicular to the growth direction ([001] direction) in order to prepare a surface parallel to the (001) plane. The specimens were mechanically polished and etched with an agent of 20 g $CuSO_4$ + 100 mL HCl + 5 mL H_2SO_4 + 80 mL H_2O for 30–40 s to deeply dissolve the γ' phase. High resolution SEM observations were performed using a HITACHI SU8010N field emission gun SEM (FE-SEM) with the secondary electron imaging mode. The characterization of the average network mesh size was conducted manually by measuring at least 200 cells per sample. For each analyzed picture, only the flattest cells of the dislocation network were included in the statistical analysis to avoid any uncertainties in the dislocation networks spacing measurement due to local curvature of the γ/γ′ interfaces.

2 Results

2.1 Phase morphology

Figure 1 shows the γ' phase morphology of DD5 alloy after standard heat treatment and long term thermal aging at 1,100 °C for different times. After standard heat treatment, the microstructure consists of cubic shape γ' phase with the size of about 400 nm and γ matrix channel with the width of about 50 nm [Fig. 1(a)]. After thermal aging at 1,100 °C for 20 h, the γ' particles coarsen and the shape of γ' particles keeps square or rectangular due to the elastic stresses [Fig.1 (b)]. The size and shape of γ' particles are uneven, some maintain cubic shape and some turn into circular shape. Some γ channels turn wider and some turn obviously thinner. Some γ' particles link to adjacent particles, and coalesce to coarsen among particles through diffusion (marked by white arrow). Moreover, except for the element diffusion, the reduction of interface energy is also the driving force for the coalescence and coarsening of γ' phase. When the aging time reaches 100

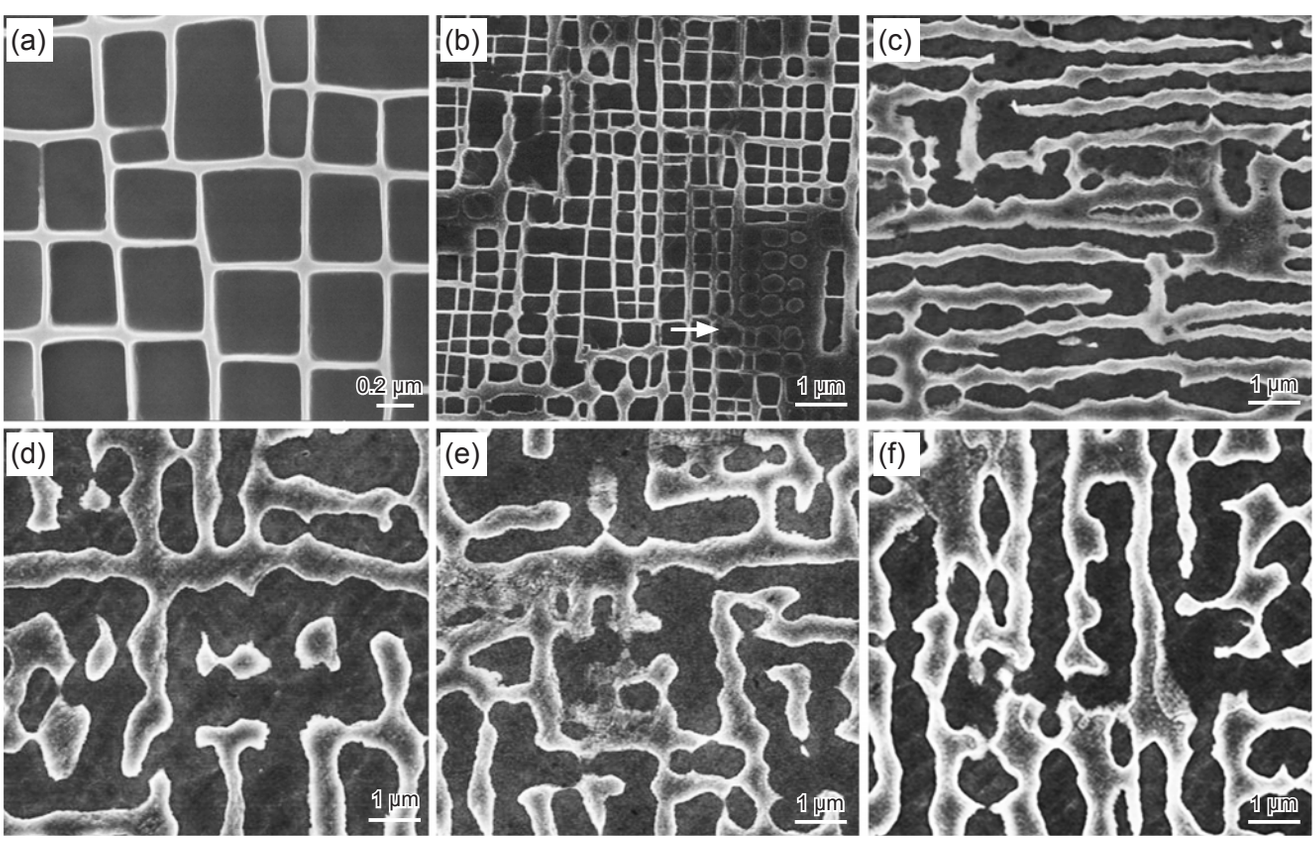

Fig. 1: Morphology of γ' phase after long term thermal aging at 1,100 °C for different times: (a) 0 h; (b) 20 h; (c) 100 h; (d) 200 h; (e) 500 h; (f) 1,000 h

h, the γ' particles are linked and rafted, as shown in Fig. 1(c). The γ channel obviously widens from 50 nm to about 300 nm. After long term aging for 200 h, the γ' particle links further along [010] or [100] direction to form the "L" shape structure and rafts. The γ matrix has been encompassed by γ' phase, as shown in Fig. 1(d), and is called topological inversion by Fredholm & Strudel [14]. With the prolonged of aging time, the γ' phase rafts in the [010] direction and the γ channel widens further to reach ~500 nm [Fig. 1 (e) and (f)].

2.2 Interfacial dislocations

A large amount of interfacial dislocations were observed in the (001) plane in the FE-SEM picture, as shown in Fig. 2. Epishin A, et al. [12] found that such semi-coherent interfaces can be visualized by scanning electron microscope (SEM) after deep etching. In the standard heat treatment specimen [Fig. 1(a)], there is almost no interfacial dislocation observed on the γ/γ' interface, which illustrates that the γ/γ' interfaces are coherent interfaces in a heat treated state. Figure 2(a) shows the interfacial dislocations in the (001) plane created by coherency strains in DD5 alloy after annealing at 1,100 °C for 20 h. The moving dislocations can be recognized by a zigzag configuration [7]. These dislocations lie at an angle of 45° to the cube face at the γ/γ' interfaces as a result of bowing through the channels on {111} planes. As the reference [15, 16] reported, this kind of dislocation is mixed dislocation, with their Burgers vectors inclined at an angle of 60° to the dislocation line. Consequently, these dislocations are at least partially relieving the misfit on the horizontal faces resulting from the different coefficients of thermal expansion between matrix and γ' phase, and compositional variation caused by dissolution of /γ' phase at high temperature.

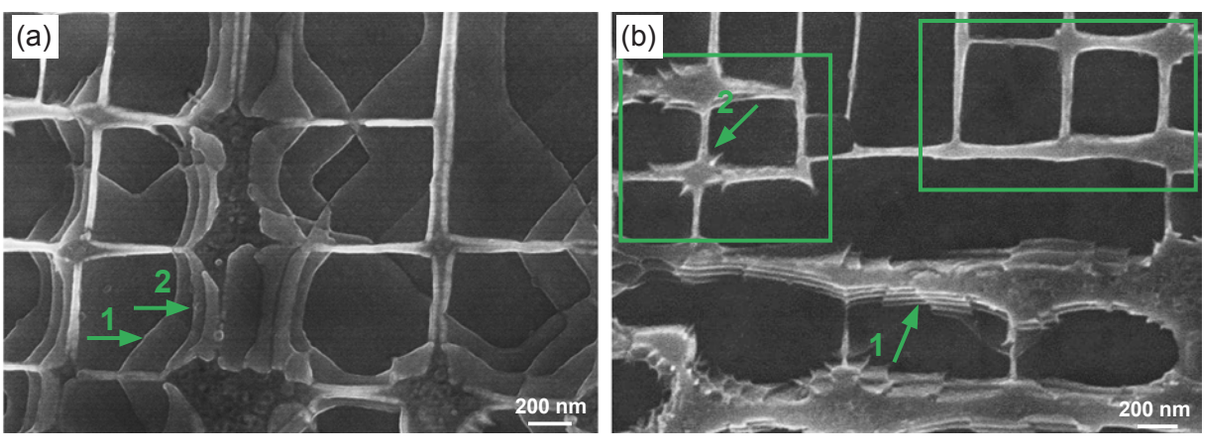

Fig. 2: Dislocation pattern of DD5 alloy after long term aging for 20 h: (a) dislocations on (001) plane; (b) dislocations perpendicular to (001) plane

The leading parts of the bowed-out dislocations move along the γ/γ' interface. It is known that the image plane is (001) plane and the edge of cube γ' phase is oriented in the [010] and [100] direction. Therefore, the line vectors of dislocation segments lying on the (001) interface can be inferred as [110] and [$\bar{1}$10] direction. Studies [6, 15] show that the motion of dislocations in γ channels is mainly determined by the Orowan resistance, misfit stress, and applied stress. While there is no applied stress in these specimens, the driving force of dislocation movement is only the misfit stress.

According to the references [12, 13], from the asymmetric contrast in the picture, the movement direction of dislocation on the interface can be inferred as the green arrows in Fig. 2(a). In some areas, it can be seen that the right-angle bends gradually straightened, and the dislocations reoriented into <100> directions by residual misfit stresses and dislocation line tension during high temperature aging [Arrows 1 and 2 in Fig. 2(a)]. Because the Burgers vector of dislocation cannot change, the 60° dislocations transform into 90° dislocations. The phenomenon of dislocations reorientation has been reported in some studies [15, 17]. The 90° dislocation is the most effective strain-relieving dislocation, which can relieve a misfit strain of $\sqrt{2}a/2$, while the 60° dislocation is less effective in strain relief, which can relieve a misfit strain of $\sqrt{2}a/4$. However, the 60° dislocation usually forms at first, because only the 60° dislocation can glide on (111) planes into the (001) interface after it has formed as a half loop from the surface [14]. When two groups of 90° dislocation from [100] and [010] directions encounter, they will intercross and form the dislocation networks. As Fig. 2(b) shows, in some areas, the γ' phase is still cubic and only a few dislocations can be found at the interface; while in some areas, the rectangular networks consisting of <001> oriented segments with a mesh size of about 200 nm have already been built, as marked by Arrow 1. Such rectangular networks were observed by Zhang et al [15, 16], which will be discussed later. If the γ/γ' interface on (001) plane cannot be observed in the specimen, the cross section of (010) and (100) plane will be seen clearly as shown in Fig. 2(b). In this kind of γ/γ' interface, there are some grooves in the matrix with sharp edges labelled by green arrow, which are the cross-section of interface dislocations. From the above, it can be inferred that the interfacial misfit dislocations occur in the corner of γ' particles first and the morphology of γ' particles will turn irregular.

Figure 3(a) and (b) shows the interfacial dislocation networks in the specimen of thermal aging for 100 h. It can be seen that the γ/γ' interfaces perpendicular to and parallel to the picture

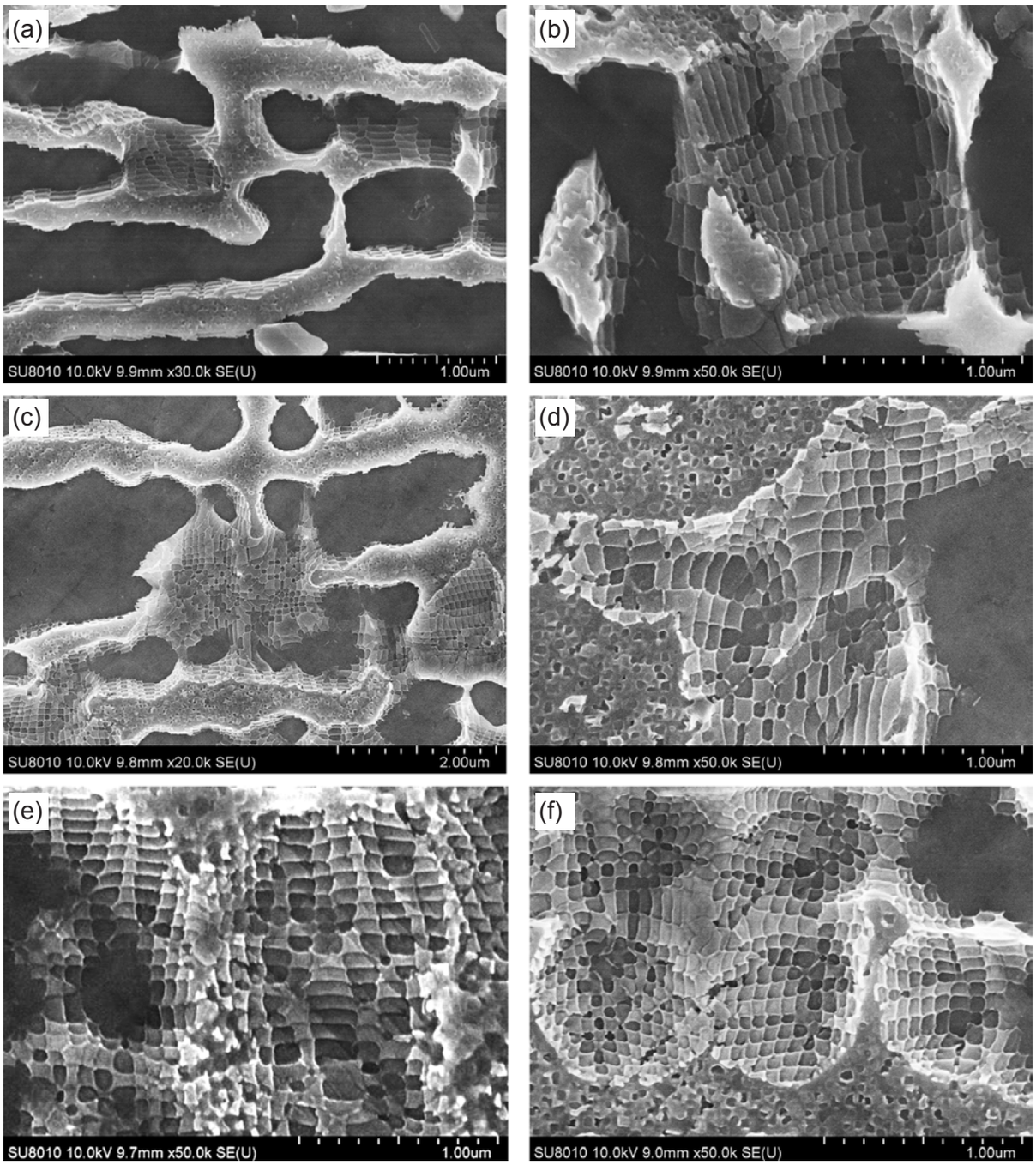

Fig. 3: Interfacial dislocation networks of DD5 alloy after long term aging for different times at 1,100 °C: (a, b) 100 h; (c, d) 200 h; (e) 500 h; (f) 1,000 h

have been covered by very dense dislocation networks after long term thermal aging for 100 h. Most of them are square or rectangular shape, but the mesh size is inhomogeneous, ranging from 100 nm to 700 nm. In all the specimens of long term aging at 1,100 °C longer than 100 h, dislocation networks can be seen in all the γ/γ' interface, as shown in Fig. 3(c–f). From Fig. 3(d–f), it can be seen that most of the dislocation networks are square or rectangular shape, and with the prolonging of aging time, the spacing of dislocation networks turns smaller and smaller.

In the 200 h specimen, except for the square and rectangular networks, there exist octagonal networks with a square node, as shown in the left side (marked by rectangular box) in Fig. 4(a). The octagonal dislocations networks also were found by TEM [6] and by SEM [12]. They all contain a small central dislocation loop, looking like a black hole, with white radial <110> segments. The distance between adjacent nodes is about 150 nm in the <001> direction. Such dislocation nodes have been found to be a dominant network in CMSX-4 and SRR99 after creep at 1,100 °C/120 MPa in Ref. [9]. With the prolonged aging time, the percentage of octagonal networks increases gradually. As shown in Fig. 4(b), taken from the specimen thermal aged for 500 h, the octagonal networks are uneven. The diameter of the central black loop varies strongly within the image from about 80 nm down to 20 nm. Figure 4(c) shows the dislocation networks of DD5 alloy after thermal aging for 500 h at 1,100 °C. In the γ/γ' interface, except for the

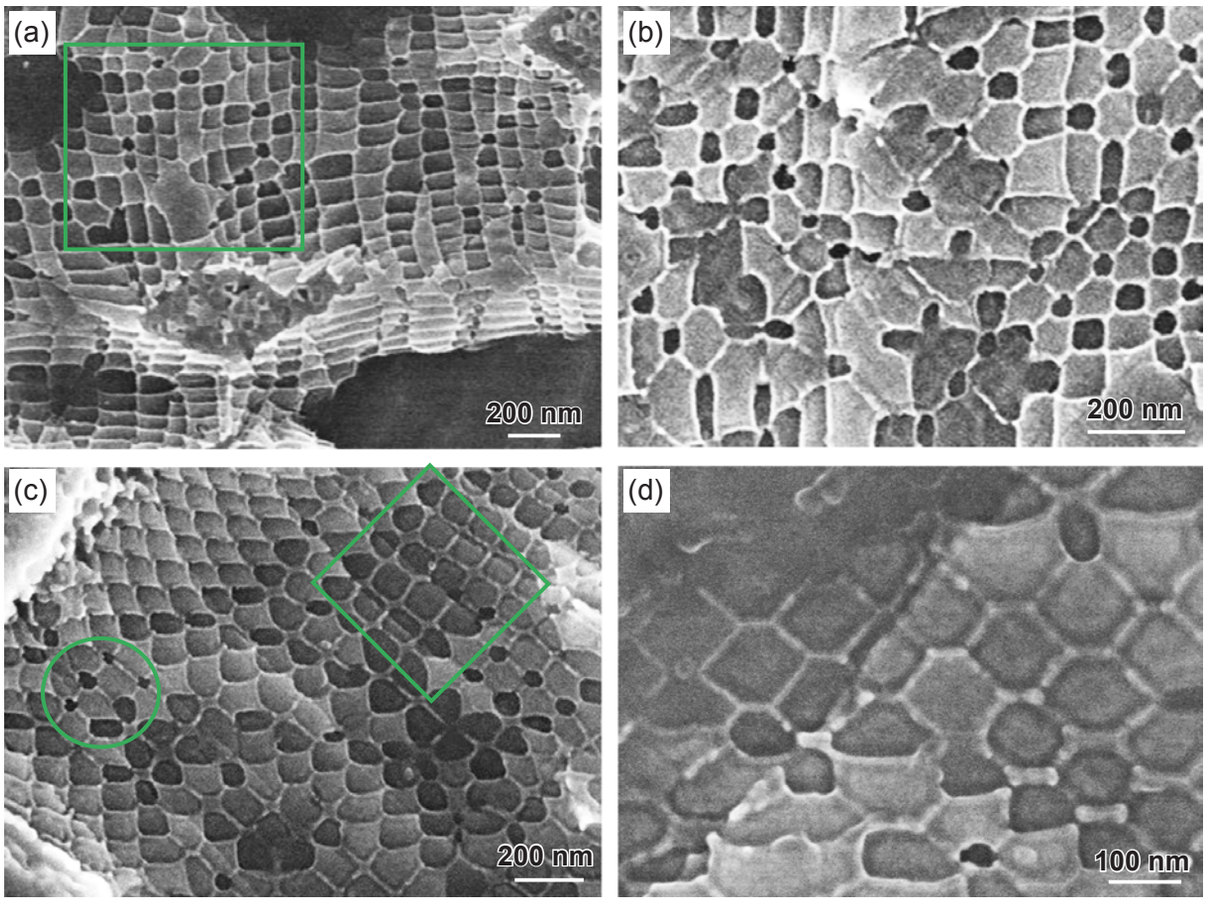

Fig. 4: Interfacial dislocation networks pattern after long term aging for different time: (a) Square and octagonal dislocation networks for 200 h; (b) Octagonal dislocation networks for 500 h; (c) Square dislocation networks for 500 h; (d) Hexagonal dislocation networks for 1,000 h

square and octagonal networks, another structure of dislocation networks was observed, as shown in Fig. 4(c) (marked by rectangle), which is regular square shape with edges along <110> direction. This kind of network is different from the initial square networks with dislocation line along the [100] and [010] direction, as shown in Fig. 3(b). The <110> dislocation segments show a completely different contrast in SEM: their image is brighter and broader than that of <100> dislocation segments in square networks. A dislocation with the above characteristics can be justified as reaction dislocation [12].

In addition, a small number of hexagonal dislocation networks were observed in the specimen of long term aging for 1,000 h [Fig. 4(d)]. This kind of hexagonal dislocation configuration is usual in high temperature creep tests [18-20], while it is unusual in long term thermal aging specimens. Xie [18] thought that the hexgonal dislocation networks are the product of two groups of dislocations with different Burgers vectors to form another dislocation; three groups of dislocations with different Burgers vectors may knit together to form the dislocation networks with a hexagonal feature. From the contrast of the dislocation lines, all the three dislocations in the hexagonal configuration can be justified as reaction dislocations, because reaction dislocation lines are brighter and wider than initial dislocation lines [12]. Therefore, the hexagonal dislocation networks are the product of another dislocations reaction, which will be discussed later.

2.3 Lattice misfit

Most commercial single crystal superalloys have a negative lattice misfit. It is well understood that the magnitude of the lattice misfit determines the density of the interfacial dislocations to relieve the misfit stress. The lattice misfit δ is defined as $\delta = (a_{\gamma'} - a_{\gamma})/a_{\gamma}$, where $a_{\gamma'}$ and a_{γ} are the lattice parameters of γ' and γ phase, respectively. Reference [21] indicated the difference between the lattice misfit and the effective lattice misfit. The lattice misfit calculated using Brook formula [22], which was based on the spacing of dislocation network, was defined as the effective lattice misfit. In the current study, the effective lattice misfit δ_{eff} had also been calculated using Brook formula, as follows:

$$\left|\delta_{\text{eff}}\right| = \frac{|b|}{d}$$

where $|b|$ and d are the magnitude of the Burgers vector and the average spacing of dislocation networks, respectively.

Therefore, the effective lattice misfit can be estimated reasonably by the average spacing of dislocations within the equilibrium interfacial networks. Different areas in each sample were examined in detail to ensure that the interfacial networks observed are representative of the studied sample. In order to make proper statistical analysis to determine the lattice misfit parameter, a large number of dislocation spacings from different

orientations was analyzed. All the dislocation networks chosen for counting are square network, as shown in Fig. 3. It can be seen that with prolonged of long term thermal aging time, the interfacial networks are denser and denser. The dislocation networks spacing turns smaller, resulting in the effective lattice misfit becoming larger. As shown in Table 1, the effective lattice misfit in the early stages increases faster than that of later stages during thermal aging at 1,100 °C.

Table 1: Dislocation networks spacing and effective lattice misfit (δ_{eff}) after thermal aging at 1,100 °C

Thermal aging time (h)	Dislocation spacing (nm)	δ_{eff}
20	240	–0.10%
100	150	–0.17%
200	100	–0.25%
500	85	–0.30%
1000	80	–0.32%

3 Discussion

3.1 γ' rafting mechanism

High temperature thermal exposure and creep of Ni-based single crystal superalloy will lead to the coalescence and rafting of γ' phase, and the grooves and ledges also form at γ/γ' interfaces. Paris et al [21] investigated the formation of serrated interfaces using two complementary methods, small-angle X-ray scattering and TEM. In our work, the serrated interface was observed using FE-SEM, as shown in Fig. 5(a). It can be seen that primary γ' particles dissolve from their corners firstly. Next to the dissolving corners, some small secondary γ' particles in the adjacent γ phase regions can be found (marked by white arrow), which is the reprecipitation of dissolved γ' phase forming element. The grooves and ledges are the cross-section of interfacial dislocations [13]. Because FE-SEM method allows us to observe large fields of view with a high resolution, a great amount of information can be obtained from the specimen. Part A in Fig. 5(b) shows cubic γ' particles where only one dislocation occurs. Whereas

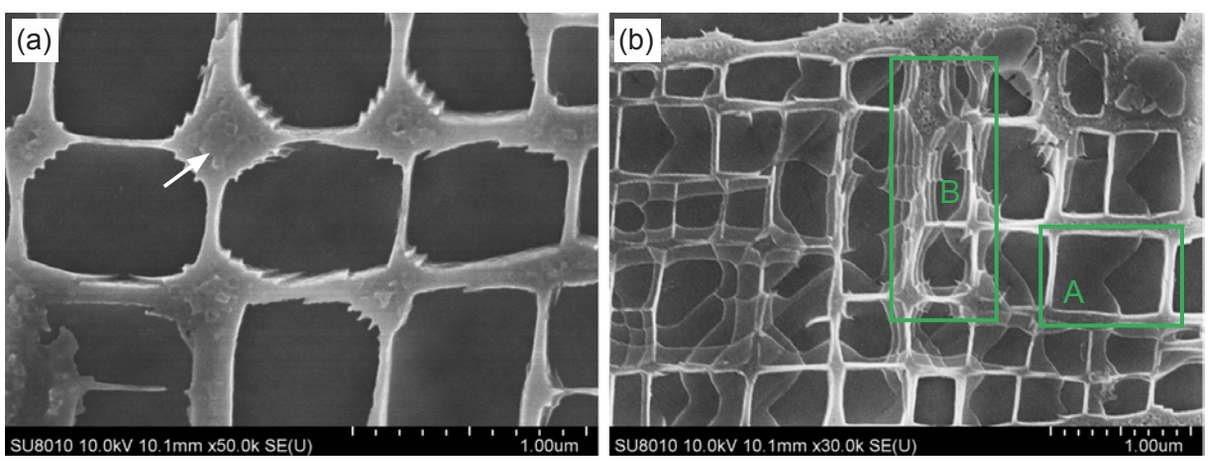

Fig. 5: Dislocation pattern of DD5 alloy after long term aging for 20 h: (a) Dislocations formed at the corner of γ' phase first; (b) Inhomogeneous dislocations on (001) plane

there are lots of dislocations and γ' has been linked in Part B, where is just hundreds of nanometer away from part A. Such pronounced microstructural differences attribute to the interfacial concentrations difference. Because particle sizes are inhomogeneous after heat treatment and many particles present obvious rectangular rather than square [13], and the interfacial concentrations would vary in virtue of particles with different sizes and shapes. In our work, the dislocation density in linking γ' phase is obviously more than that of single γ' particle. When the aging time reaches 100 h, the rafts form [Fig. 1(c)] and the γ/γ' interface has been covered by very dense dislocation networks [Fig. 3(a)]. All the above phenomena illustrated that the interfacial dislocation can accelerate the rafting process. Paris O, et al [23-25] underlined in their research results the importance of the presence of dislocations at γ/γ' interfaces during rafting. No case has been documented where rafting occurs in the absence of dislocations.

3.2 Formation mechanism of dislocation networks

Interfacial dislocation networks have been observed and analyzed by TEM [12-15]. Although the Burgers vectors of dislocations cannot be identified directly by SEM, the possible vectors can be inferred by the given geometrical relationship. Because the observed specimen surface is (001) plane perpendicular to the growth direction of [001] and the edges of cube γ' are [010] and [100] direction, according to the zone law, the Burgers vectors of 90° dislocations in this work with [100] line vectors should be a/2[011] or a/2[01$\bar{1}$]; the Burgers vectors of dislocations with [010] line vector should be a/2[101] or a/2[10$\bar{1}$]. According to the stereographic microscope analysis, the dislocation lines lie approximately along the [010] or [100] direction in the relatively regular square areas. Different groups of a/2<110> dislocations intersect to form the square or rectangular networks, as shown in Fig. 6. They can form five types of

dislocation networks by the reactions of Eqs. (1) to (4). If two groups of dislocations react as Eq. (1) or (4), the dislocation network configuration as shown in Fig. 6(a) can form and the a/2[110] dislocation segments occur, which were named as A type dislocation networks. If two groups of dislocations react as Eq. (2) or (3), the dislocation network configuration as shown in Fig. 6(b) can form and the a/2[1$\bar{1}$0] dislocation segment occurs, which was named as B type dislocation networks. When three groups of dislocation take part in the reaction, the networks will occur, as shown in Fig. 6(c), which were named as C type dislocation networks. Four groups of dislocations can form D or E type dislocation networks, as shown in Fig. 6(d) and (e), where the brown and black dislocation segments have the Burgers vector of a/2[110] and a/2[1$\bar{1}$0]. All the reactions above result in a reduction in b^2 from a^2 to $1/2a^2$ (where a is the lattice constant), and thus these would be energetically favorable.

At the early stage of all the dislocation networks formation, it is difficult to distinguish the five types of dislocation networks, because the reaction segments are so short that they all belong

$$\frac{1}{2}[011]+\frac{1}{2}[10\bar{1}]\rightarrow\frac{1}{2}[110] \quad (1)$$

$$\frac{1}{2}[011]+\frac{1}{2}[\bar{1}0\bar{1}]\rightarrow\frac{1}{2}[\bar{1}10] \quad (2)$$

$$\frac{1}{2}[01\bar{1}]+\frac{1}{2}[\bar{1}01]\rightarrow\frac{1}{2}[\bar{1}10] \quad (3)$$

$$\frac{1}{2}[01\bar{1}]+\frac{1}{2}[101]\rightarrow\frac{1}{2}[110] \quad (4)$$

to square or rectangular networks. However, with the thermal aging time prolonged, the reaction continues to proceed and the type of dislocation networks can be distinguished easily. There are three types of dislocation networks in Fig. 7(a), which are A, B and C type, respectively, where the reaction dislocation segment can be seen clearly as highlighted with small black line segments. In addition, with the further development of dislocation reaction, D type dislocation networks can transform into the configuration, as shown in Fig. 6(d), whose dislocation

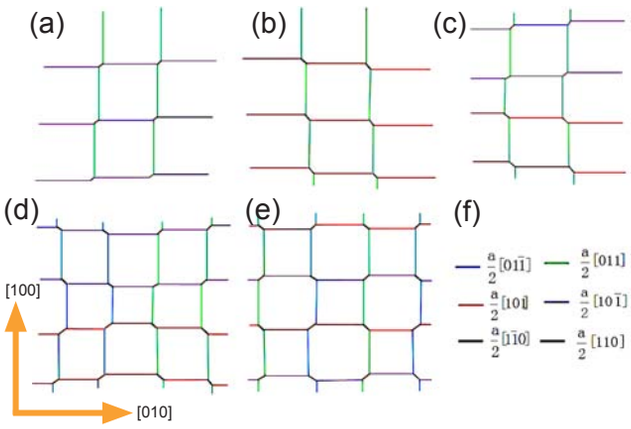

Fig. 6: Schematic diagram for different types of square interfacial dislocation networks: (a) type A; (b) type B; (c) type C; (d) type D; (e) type E; (f) graphic symbols (Burgers vectors of dislocations)

pattern has been shown in Fig. 7(b). E type dislocation network in Fig. 6(e) can transform into the octagonal dislocation network with a square node, as shown in Fig. 8(a). From the contrast in SEM image, the movement direction of dislocation can be confirmed, that is, it will move from the lighter area to the darker area. The diameter of the black loop in the octagonal network becomes smaller and smaller until it shrinks to zero, and forms the square networks in Fig. 8(b). The remaining black loop in Fig. 4(c) (marked by circle) is the best evidence.

As being pointed above, the hexagonal dislocation networks are the product of dislocations reaction. A rectangular dislocation network consisting of four groups of dislocations can react by Eqs. (1) to (4) as illustrated in Fig. 9. The Burgers vectors of A, B dislocations were determined to be a [100] by Eq. (5), which is an edge type dislocation. Four other dislocations are clearly identified by Eqs. (1) to (4), respectively. The [100] segment dislocation was also observed by Hantcherli[6]. However, Eq. (5) can satisfy the geometric conditions of the dislocation reaction, but it doesn't satisfy the energy condition of a dislocation reaction. For a stress-free specimen, the reaction should not take place. However, in a singe crystal superalloy with γ/γ' phase

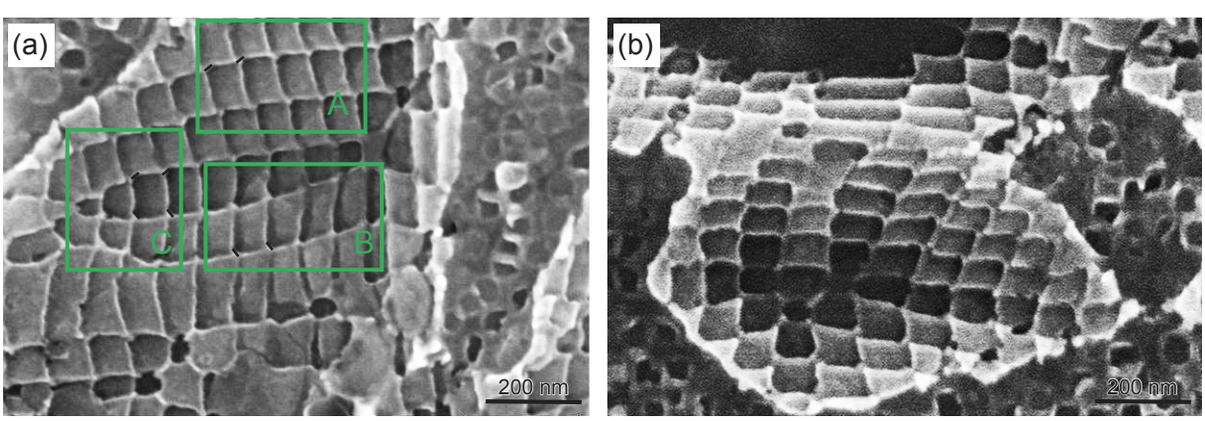

Fig. 7: Dislocation pattern of different types of square dislocation networks: (a) Dislocation networks include type A, B and C; (b) Type D square dislocation networks

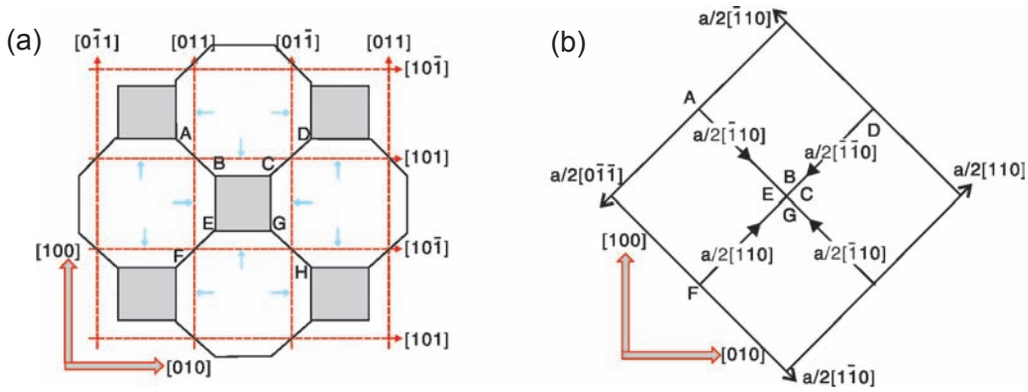

Fig. 8: Schematic diagrams of octagonal dislocation networks (a) and another square dislocation networks (b) (note: the vectors labeled in the figure are Burgers vectors)

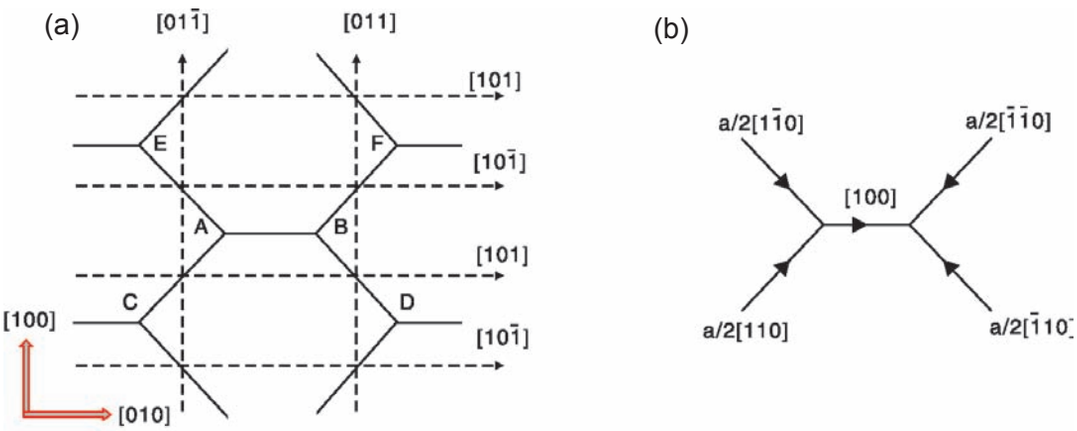

Fig. 9: Schematic diagrams of hexagonal dislocation networks (note: the vectors labeled in the figure are Burgers vectors)

microstructure [26, 27], there exist some internal stress in γ' and γ channel, which can promote the dislocation reaction.

$$\frac{a}{2}[101]+\frac{a}{2}[10\bar{1}]\rightarrow a[100] \quad (5)$$

4 Conclusion

The interfacial misfit dislocations in DD5 single crystal superalloys were observed and analyzed comprehensively by FE-SEM during long term thermal aging at 1,100 °C. In the early stage of aging, the misfit dislocations form and then reorientation in the (001) interfacial planes occurs, away from the line vector of <110> to <100> direction. Different types of square or rectangular dislocation networks will form by dislocation reaction. With prolonged thermal aging time, square dislocation networks consisting of four groups of dislocations can transform into octagonal dislocation networks, and then form other square dislocation networks by dislocation reaction. Rectangular dislocation networks consisting of four groups of dislocations can also transform into hexagonal dislocation networks. The interfacial dislocation networks promote the γ' phase rafting process. The dislocation networks spacing turns smaller and smaller, leading to the effective lattice misfit increasing from -0.10% to -0.32%

References

[1] Tang S, Ning L K, Xin T Z, et al. Coarsening Behavior of Gamma Prime Precipitates in a Nickel Based Single Crystal Superalloy. Journal of Materials Science & Technology, 2016, 32(2): 172–176.

[2] Tan X P, Liu J L, Song X P, et al. Measurements of gamma/gamma' Lattice Misfit and gamma' Volume Fraction for a Ru-containing Nickel-based Single Crystal Superalloy. Journal of Materials Science & Technology, 2011, 27(10): 899–905.

[3] R.C. Reed, The superalloys: Fundamentals and Applications. Cambridge, 2008.

[4] Tang S, Zheng Z, Ning L K. Gamma prime coarsening in a nickel base single crystal superalloy. Materials Letters, 2014, 128: 388–391.

[5] Liu L R, Jin T, Zhao N R, et al. Microstructural evolution of a single crystal nickel-base superalloy during thermal exposure. Materials Letters, 2003, 57(29): 4540–4546.

[6] Hantcherli M, Pettinari-Sturmel F, Viguier B, et al. Evolution of interfacial dislocation network during anisothermal high-temperature creep of a nickel-based superalloy. Scripta Materialia, 2012, 66(3–4): 143–146.

[7] Zhang J X, Murakumo T, Koizumi Y, et al. The influence of interfacial dislocation arrangements in a fourth generation single crystal TMS-138 superalloy on creep properties. Journal of Materials Science, 2003, 38(24): 4883–4888.

[8] Feller-Kniepmeier M, Link T. Dislocation structures in γ-γ′ interfaces of the single-crystal superalloy SRR 99 after

annealing and high temperature creep. Materials Science & Engineering A, 1989, 113: 191–195.
[9] Field R D, Pollock T M, Murphy W H, et al. Superalloys 1992. TMS, Warrendale, PA557, 1992.
[10] Pollock T M, Argon A S. Creep Resistance of CMSX-3 Nickel Base Superalloy Single Crystals. Acta Metallurgica Et Materialia, 1992, 40(1): 1–30.
[11] Zhang J X, Murakumo T, Koizumi Y, et al. Slip geometry of dislocations related to cutting of the γ′ phase in a new generation single-crystal superalloy. Acta Materialia, 2003, 51(17): 5073–5081.
[12] Epishin A, Link T, Nolze G. SEM investigation of interfacial dislocations in nickel-base superalloys. Journal of Microscopy (Oxford), 2007, 228(2): 110–117.
[13] Link T, Epishin A, Paulisch M, et al. Topography of semicoherent γ/γ′-interfaces in superalloys: Investigation of the formation mechanism. Materials Science & Engineering A, 2011, 528(19): 6225–6234.
[14] Fredholm A, Strudel J L. High Temperature Creep Mechanisms in Single Crystals of Some High Performance Nickel Base Superalloys//High Temperature Alloys. Springer Netherlands, 1987.
[15] Zhang J X, Harada H, Koizumi Y, et al. Dislocation motion in the early stages of high-temperature low-stress creep in a single-crystal superalloy with a small lattice misfit. Journal of Materials Science, 2010, 45(2): 523–532.
[16] Chen Y, Lilientalweber Z, Washburn J, et al. Reorientation of misfit dislocations during annealing in InGaAs/GaAs(001) interfaces. Mrs Proceedings, 1993, 308: 12–16.
[17] Zhang J X, Wang J C, Harada H, et al. The effect of lattice misfit on the dislocation motion in superalloys during high-temperature low-stress creep. Acta Materialia, 2005, 53(17): 4623–4633.
[18] Xie J, Tian S, Shang L J, et al. Creep behaviors and role of dislocation network in a powder metallurgy Ni-based superalloy during medium-temperature. Materials Science and Engineering: A, 2014, 606: 304–312.
[19] Zhang J X, Murakumo T, Koizumi Y, et al. Interfacial dislocation networks strengthening a fourth-generation single-crystal TMS-138 superalloy. Metallurgical and Materials Transactions A (Physical Metallurgy and, Materials Science), 2002, 33(12): 3741–3746.
[20] Boualy O, Clément N, Benyoucef M. Analysis of dislocation networks in crept single crystal nickel-base superalloy. Journal of Materials Science, 2018, 53(4): 2892–2900.
[21] Yue Q Z, Liu L, Yang W C, et al. Stress dependence of dislocation networks in elevated temperature creep of a Ni-based single crystal superalloy. Materials Science & Engineering A, 2019, 742: 132–137.
[22] Dirand L, Cormier J, Jacques A, et al. Measurement of the effective γ/γ′ lattice mismatch during high temperature creep of Ni-based single crystal superalloy. Materials Characterization, 2013, 77: 32–46.
[23] Paris O, Fa¨hrmann M, Fa¨hrmann E, et al. Early stages of precipitate rafting in a single crystal NiAlMo model alloy investigated by small-angle X-ray scattering and TEM. Acta Materialia, 1997, 45(3): 1085–1097.
[24] Vorontsov V A, Kovarik L, Mills M J, et al. High-resolution electron microscopy of dislocation ribbons in a CMSX-4 superalloy single crystal. Acta Materialia, 2012, 60(12): 4866–4878.
[25] Kolbe M, Dlouhy A, Eggeler G. Dislocation reactions at γ/γ′-interfaces during shear creep deformation in the macroscopic crystallographic shear system (001)[110] of CMSX6 superalloy single crystals at 1025°C. Materials Science & Engineering A, 1998, 246(1–2): 133–142.
[26] Pollock T M, Argon A S. Directional coarsening in nickel-base single crystals with high volume fractions of coherent precipitates. Acta Metallurgica et Materialia, 1994, 42(6): 1859–1874.
[27] Kamaraj M, Mayr C, Kolbe M, et al. On the influence of stress state on rafting in the single crystal superalloy CMSX-6 under conditions of high temperature and low stress creep. Scripta Materialia, 1998, 38(4): 589–594.

This work was supported by the National Natural Science Foundation of China (Grant No.: 50901046).